



Relativistic equilibrium fluid configurations around rotating deformed compact objects

Shokoufe Faraji^{1,a}, Audrey Trova^{1,b}, Hernando Quevedo^{2,3,c}

¹ Center of Applied Space Technology and Microgravity (ZARM), University of Bremen, 28359 Bremen, Germany

² Instituto de Ciencias Nucleares, Universidad Nacional Autónoma de México, AP 70543, 04510 Mexico City, Mexico

³ Dipartimento di Fisica and ICRANet, Università di Roma “La Sapienza”, 00185 Rome, Italy

Received: 30 August 2022 / Accepted: 23 November 2022 / Published online: 20 December 2022
© The Author(s) 2022

Abstract The main goal of this paper is to investigate the physical properties of equilibrium sequences of non-self-gravitating surfaces that characterize Thick disks around a rotating deformed compact object described by a stationary generalization of the static q-metric. The space-time corresponds to an exact solution of Einstein’s field equations so that we can perform the analysis for arbitrary values of the quadrupole moment and rotation parameter. To study the properties of this disk model, we analyze bounded trajectories in this space-time. Further, we find that depending on the values of the parameters, we can have various disk structures that can easily be distinguished from the static case and also from the Schwarzschild background. We argue that this study may be used to evaluate the rotation and quadrupole parameters of the central compact object.

1 Introduction

The gravitational field of astrophysical compact objects can be characterized by means of their multipole moments. In Newtonian gravity, only the mass is a source of gravity and, therefore, all the multipole moments are determined by the mass distribution only. In the case of relativistic objects, there are two different sets of multipoles, namely, mass and angular momentum multipoles [1–3].

From the point of view of their multipole structure, the simplest relativistic compact objects are black holes because they can be completely characterized by the lowest possible moments, i.e., by the mass monopole and the angular momentum dipole, which determine uniquely the corresponding

Schwarzschild and Kerr space-times, respectively [4]. This is one of the essential aspects of the black hole uniqueness theorems [5].

In the case of a non-rotating mass distribution, the next non-trivial multipole is the quadrupole, which describes the deviation of the mass distribution from spherical symmetry, but preserving the axial symmetry. In this case, no uniqueness theorems exist and so there are several possibilities to describe a space-time of a mass with quadrupole. In [6], it was established that there are six different known solutions of Einstein equations that could be used to describe the gravitational field of a mass with quadrupole. From all of them, we highlight the quadrupolar metric (q-metric) as the simplest generalization of the Schwarzschild space-time, including a quadrupole [7]. The q-metric can be obtained by applying a Zipoy–Voorhees transformation [8,9] to the Schwarzschild metric and in spherical coordinates reads

$$ds^2 = - \left(1 - \frac{2m}{r}\right)^{1+q} dt^2 + \left(1 - \frac{2m}{r}\right)^{-1-q} \left(\frac{r^2 - 2mr + m^2 \sin^2 \theta}{r^2 - 2mr}\right)^{-q(2+q)} dr^2 + \left(1 - \frac{2m}{r}\right)^{-q} r^2 (d\theta^2 + \sin^2 \theta d\phi^2), \quad (1)$$

where m and q are the mass and quadrupole parameters, respectively.

The q-metric has been used to study the motion of test particles, accretion disks, black hole mimickers, shadows, interior and exterior counterparts, quasi periodic oscillations among others [10–19]. From these studies, it follows that the q-metric satisfies all the physical conditions to describe the field of a deformed mass distribution with quadrupole.

The next interesting physical aspect of compact objects is their rotation. Therefore, in the present work, as the next step of this work [16], we will consider a stationary generalization of the q-metric that contains an additional parameter,

^a e-mail: shokoufe.faraji@zarm.uni-bremen.de (corresponding author)

^b e-mail: audrey.trova@zarm.uni-bremen.de

^c e-mail: quevedo@nucleares.unam.mx

corresponding to the dipole of the angular momentum [20]. We explore the applicability of the stationary q-metric in astrophysical situations, we study the Thick accretion disk model, which is situated on the background of a rotating, deformed mass distribution. This hydrostatic equilibrium are strongly believed to form around X-ray binaries, active galactic nuclei, and also in the central engine of gamma-ray bursts. The analytical Thick disk model for an accretion disk is initially assumed to consist of an unmagnetised perfect fluid with constant angular momentum [21–28]. In this work we consider this analytical model and explain it briefly in Sect. 4.

The space-time contains three independent multipoles, namely, mass monopole and quadrupole, and angular momentum dipole. We will show that the structure of accretion disks around the stationary q-metric depends explicitly on the values of all the independent parameters of the metric. In particular, we will see that the behavior of the accretion disks agrees with our physical expectations. We also compare our results with those obtained previously for the Kerr spacetime [29–36], in particular, in the case of naked singularities.

This work is organized as follows. In Sect. 2, we present the stationary q-metric. In Sect. 3, we study some of the physical properties of the stationary q-metric. In Sect. 4, we discuss the main theoretical aspects of the Thick disk model and present the results in the space-time described by the stationary q-metric. In Sect. 5, we discuss our results. Throughout this work, the signature of the metric is set to be $(-, +, +, +)$ and we use geometrical units with $c = G = 1$.

2 The stationary q-metric

A stationary generalization of the static Zipoy–Voorhees space-time is contained as a particular solution of the rotating Erez–Rosen solution and was first presented in [37]. However, the physical meaning of the Zipoy–Voorhees parameter δ as a quadrupole parameter was first established and investigated only later on in [7]. It was named q-metric to emphasize the role of the q parameter as a quadrupole and as a source of naked singularities. The Ernst potential of the corresponding stationary generalization was presented in [20] and the explicit form of the metric was calculated in [38]. In prolate spheroidal coordinates (t, x, y, ϕ) , the corresponding line element can be written as

$$\begin{aligned}
 ds^2 = & -f(dt - \omega d\phi)^2 \\
 & + \frac{\sigma^2}{f} \left[e^{2\gamma}(x^2 - y^2) \left(\frac{dx^2}{x^2 - 1} + \frac{dy^2}{1 - y^2} \right) \right. \\
 & \left. + (x^2 - 1)(1 - y^2)d\phi^2 \right], \tag{2}
 \end{aligned}$$

where σ is a constant with the dimension of length and the metric functions depend only on x and y ,

$$\begin{aligned}
 f &= \frac{A}{B}, \\
 \omega &= -2 \left(a + \sigma \frac{C}{A} \right), \\
 e^{2\gamma} &= \frac{1}{4} \left(1 + \frac{m}{\sigma} \right)^2 \frac{A}{(x^2 - 1)^{1+q}} \left[\frac{x^2 - 1}{x^2 - y^2} \right]^{(1+q)^2}. \tag{3}
 \end{aligned}$$

Here q represents the quadrupole parameter and a is related to the angular momentum. Besides

$$\begin{aligned}
 A &= a_+ a_- + b_+ b_-, \\
 B &= a_+^2 + b_+^2, \\
 C &= (x + 1)^q [x(1 - y^2)(\lambda + \eta)a_+ + y(x^2 - 1)(1 - \lambda\eta)b_+], \tag{4}
 \end{aligned}$$

and

$$\begin{aligned}
 a_{\pm} &= (x \pm 1)^q [x(1 - \lambda\eta) \pm (1 + \lambda\eta)], \\
 b_{\pm} &= (x \pm 1)^q [y(\lambda + \eta) \mp (\lambda - \eta)], \\
 \lambda &= \alpha(x^2 - 1)^{-q}(x + y)^{2q}, \\
 \eta &= \alpha(x^2 - 1)^{-q}(x - y)^{2q}, \\
 \alpha &= \frac{1}{a}(\sigma - m).
 \end{aligned}$$

The functions f and ω are related to the twist scalar Ω through

$$f^2 \nabla \omega = \rho \phi \times \nabla z, \tag{5}$$

where

$$\rho = \sigma \sqrt{(x^2 - 1)(1 - y^2)} \text{ and } z = \sigma xy.$$

Because of the symmetries of the metric one can easily find the existing conserved quantities related to the particle motion, which are the covariant energy E and axial angular momentum L associated to the Killing vectors ∂_t and ∂_ϕ , respectively. Prolate spheroidal coordinates are used for investigating the symmetries of the field equations of stationary and axisymmetric gravitational fields [39]. Also, they allow us to express particular solutions in a very symmetric way, as in the above example. Nevertheless, for comparison with other special cases and the investigation of the physical properties of the spacetime, it is convenient to use spherical coordinates (t, r, θ, ϕ) , which are determined by the simple transformation

$$x = \frac{1}{\sigma}(r - m), \quad y = \cos \theta. \tag{6}$$

In these coordinates, the general line element (2) becomes

$$\begin{aligned}
 ds^2 = & -f(dt - \omega d\phi)^2 \\
 & + \frac{1}{f} \left[e^{2\gamma}(r^2 - 2mr + m^2 + \sigma^2 \cos^2 \theta) \right.
 \end{aligned}$$

$$\times \left(\frac{dr^2}{r^2 - 2mr + m^2 - \sigma^2} + d\theta^2 \right) + (r^2 - 2mr + m^2 - \sigma^2) \sin^2 \theta d\phi^2 \Big]. \tag{7}$$

In the limiting case $\sigma = m, \alpha = 0$, and $a = 0$, the above solution reduces to the static q-metric given in Eq. (1). Moreover, for $q = 0$, the above solution is stationary with a representing the specific angular momentum of the source. In the general stationary case, the relation with the Kerr solution is obtained by choosing the parameters as

$$\sigma = \frac{m(1 - \alpha^2)}{(1 + \alpha^2)}, \tag{8}$$

$$a = \frac{-2\sigma\alpha}{(1 - \alpha^2)}, \tag{9}$$

so that

$$\sigma^2 = m^2 - a^2. \tag{10}$$

In the following analysis, we will use spherical coordinates (t, r, θ, ϕ) ; nevertheless, in some equations, we will use the coordinates x and y for simplicity reasons.

It is convenient to consider m and a as the independent parameters, instead of σ and α . Indeed, by setting $a = 0$, we obtain the limiting case of the static q-metric. Moreover, for $q = 0$, the above solution is stationary with a representing the specific angular momentum of the source. Figure 1 shows the relationship of the rotation parameter a with σ and α , respectively. In general, parameter q describes how the mass distribution along an axis is stretched out. It can be zero, positive or negative, corresponding to a sphere, an prolate or an oblate mass distribution, respectively.

3 Physical properties of the stationary q-metric

In this section, we investigate the main physical properties of the stationary q-metric and the particular spacetimes that are contained as limiting cases by using an invariant definition of multipole moments. We also investigate the behavior of the Ernst potential, which contains all the main information about the metric of the corresponding spacetime, and the conditions for the existence of bounded and circular geodesics.

3.1 Multipole moments

In general, the physical meaning of the parameters entering the metric can be clarified by calculating the relativistic multipole moments [1–3, 38]. By using the Geroch–Hansen relativistic coordinate-invariant definition of multipole moments, we obtain

$$M_0 = m + \mathcal{X}, \tag{11}$$

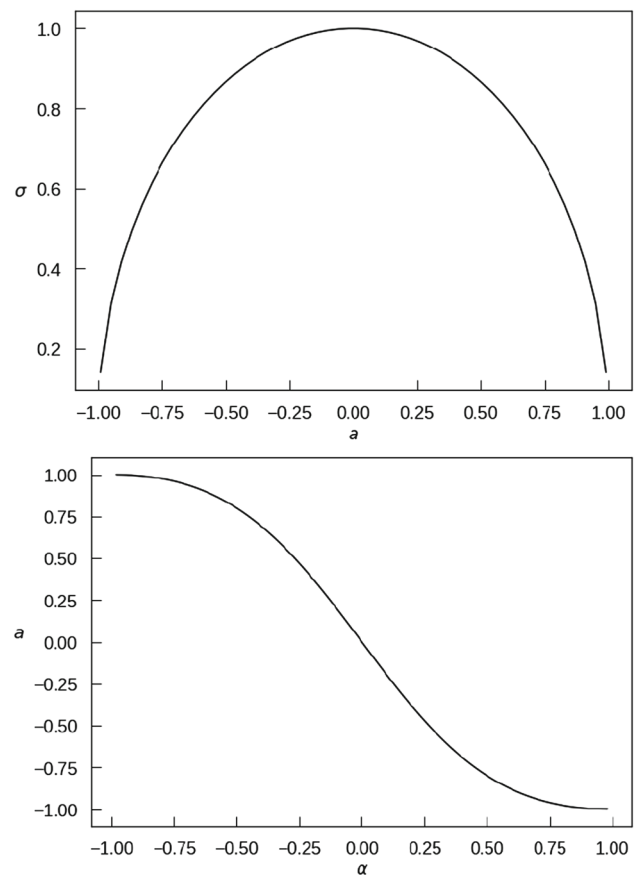


Fig. 1 The rotation parameter a as a function of the parameters σ and α with $m = 1$

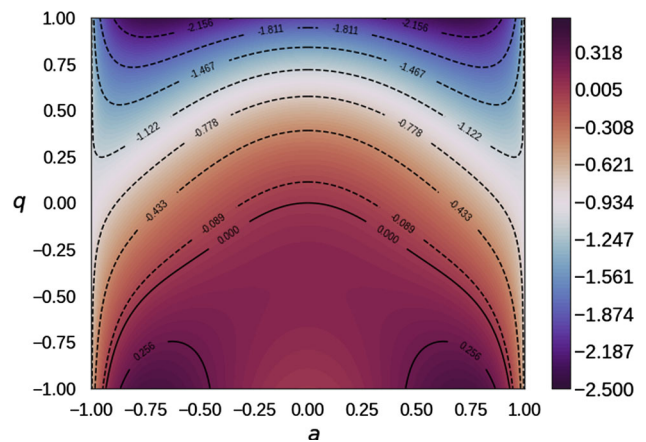


Fig. 2 The behavior of the relativistic quadrupole M_2 for different parameters a and q

$$J_1 = ma + 2a\mathcal{X}, \tag{12}$$

$$M_2 = -m^3 + m\sigma^2 + \left(\frac{7}{3}\sigma^2 - 3m^2\right)\mathcal{X} - m\mathcal{X}^2 - \frac{1}{3}\mathcal{X}^3, \tag{13}$$

where $\mathcal{X} := q\sigma$. All the higher moments can be expressed in terms of the above multipoles. Moreover, all the odd mass

moments M_{2k+1} and even angular momentum moments J_{2k} vanish identically as a result of the existing reflection symmetry with respect to the equatorial plane.

Since all the higher multipole moments can be written in terms of the first and second multipoles, from the above expressions for the relativistic multipole moments, we see that the three parameters m , q , and a that enter the metric are present in the expressions for all multipoles through the quantity \mathcal{X} .

To illustrate the dependence of the multipoles from the independent parameters, we plot in Fig. 2 the behavior of the relativistic quadrupole M_2 . We see that M_2 is symmetric with respect to the value of a , but no symmetry exists with respect to the parameter q . This is due to the fact that in this case the gravitational field does not depend on the direction of rotation, whereas the sign of quadrupole q determines the shape of the source, which can be either prolate or oblate, corresponding to different gravitational fields.

The limiting cases of the stationary q-metric can also be studied from the expressions of the multipole moments. Indeed, for $a = 0$, from the above expressions we obtain

$$M_0 = m(1 + q), \tag{14}$$

$$J_1 = 0, \tag{15}$$

$$M_2 = -\frac{m^3}{3}(q^3 + 3q^2 + 2q), \tag{16}$$

which are the multipoles of the static q-metric [7]. If, in addition, we set $q = 0$, we obtain that the only non-vanishing multipole is the monopole, $M_0 = m$, i.e., we obtain the multipole structure of the Schwarzschild spacetime. Notice also that in the additional limit $q = -1$, all the multipoles vanish, indicating that no gravitational source exists. This can also be verified by calculating the curvature of the q-metric.

Consider now the limiting case of a vanishing quadrupole parameter, $q = 0$. Then, from the above expressions for the multipoles we get

$$M_0 = m, \quad J_1 = ma, \quad M_2 = -ma^2, \tag{17}$$

which coincide with the multipoles of the Kerr metric [3,37], where m is the total mass and $a = J_1/m$ is the specific angular momentum. From a physical point of view, the rotation generates an oblate deformation of the gravitational source, which in this case is described by the quadrupole moment $M_2 = -ma^2$. Therefore, it is usually assumed as a convention that an oblate deformation of the source corresponds to a negative value of the quadrupole moment.

It is interesting to mention the limit $m = a$, for which we obtain the following expressions for the multipoles

$$M_0 = m, \quad J_1 = m^2, \quad M_2 = -m^3, \tag{18}$$

which coincide with the Kerr multipoles (17) for $a = m$, i.e., with the multipoles of the extreme Kerr black hole. Therefore,

the stationary q-metric in the limit of $m = a$ describes the gravitational field of an extreme rotating black hole, independently of the value of the quadrupole parameter q . A similar behavior has been found in generalizations of the Kerr spacetime with other metrics with quadrupole and higher multipole moments [37].

We thus conclude that the stationary q-metric is a generalization of the static q-metric, which contains the Kerr spacetime as a particular case, in the limit of a vanishing quadrupole parameter, and reduces to the metric of an extreme black hole when the rotational parameter coincides in value with the mass parameter, independently of the value of the quadrupole.

3.2 The Ernst potential

To further analyze the physical meaning of the stationary q-metric, we consider the corresponding Ernst potential which for stationary vacuum fields is defined as [40,41]

$$\mathcal{E} = f + iz, \tag{19}$$

where the function z is determined by the following equations

$$\sigma(x^2 - 1)z_x = f^2\omega_y, \tag{20}$$

$$\sigma(1 - y^2)z_y = -f^2\omega_x. \tag{21}$$

where σ is the constant entering the spatial part of the metric, and f and ω are the metric functions. Thus, once we have \mathcal{E} , the function f can be found algebraically and ω follows from the above equations. This implies that the Ernst potential contains all the information about f and ω , which are the main metric functions, whereas the metric function γ can be obtained by quadratures from the explicit value of f and ω [40,41]. Therefore, from a given Ernst potential one can derive the explicit value of the metric, i.e., all the information about the corresponding gravitational field. For instance, from \mathcal{E} we can extract information about the asymptotic behavior of the metric. In particular, the q-metric can be shown to be asymptotically flat [7]. The corresponding Ernst potential for the stationary q-metric is obtained by utilizing the solution generating techniques [20,39] as follows

$$\mathcal{E} = \left(\frac{x-1}{x+1}\right)^q \left[\frac{x-1+(x^2-1)^{-q}d_+}{x+1+(x^2-1)^{-q}d_-} \right], \tag{22}$$

where

$$d_{\pm} = -\alpha^2(x \pm 1)h_+h_-(x^2 - 1)^{-q} + i\alpha[y(h_+ + h_-) \pm (h_+ - h_-)], \tag{23}$$

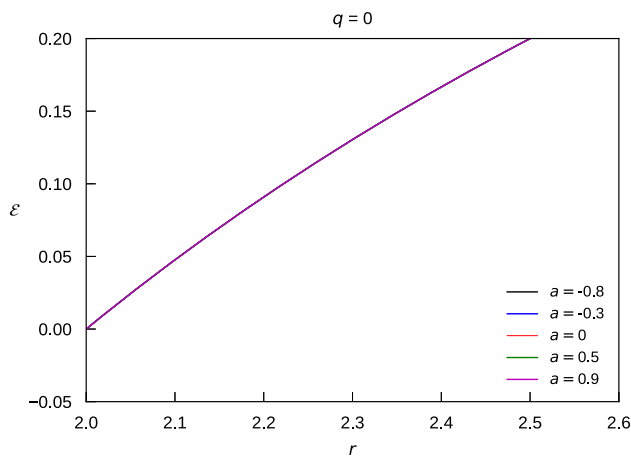


Fig. 3 The Ernst potential on the equatorial plane for vanishing q and different spin parameters a

and

$$h_{\pm} = (x \pm y)^{2q}. \tag{24}$$

In Figs. 3 and 4, we study the behavior of the Ernst potential on the equatorial plane $\theta = \pi/2$ ($y = 0$) as a function of the radial coordinate r for different values of the two independent parameters q and a .

In the case $q = 0$, the Ernst potential reduces to

$$\mathcal{E} = \frac{a^2(x - 1) - (\sigma - m)^2(x + 1)}{a^2(x + 1) - (\sigma - m)^2(x - 1)}. \tag{25}$$

Since $|a| \in [0, 1)$, its square is a small quantity. Also, the coefficients of a^2 in the numerator and denominator of the Ernst potential (25) are of the same order and comparable, i.e., the values of \mathcal{E} for different values of a are very close to each other. The result is shown in Fig. 3. We can see that for each value of a , the Ernst potential is a continuous function of r that tends monotonically to a constant at infinity. However, when we plot the Ernst potential for different values of $q \neq 0$, as shown in Fig. 4, we notice that there are certain points at which the Ernst potentials for different values of a coincide. Since the Ernst potential contains all the information about the gravitational field, we conclude that at the intersection points the corresponding space-times are identical. A detailed numerical analysis of the intersection points shows that they are located close to the radius value $r = 2m$, i. e., close to the outermost singularity, as we will see below.

3.3 Curvature singularities

We also investigated the position of the curvature singularities of the stationary q -metric. In fact, for the static q -metric (1) it was shown in [7] that there exist an exterior singularity located at $r = 2m$ and an interior singularity with $r < 2m$

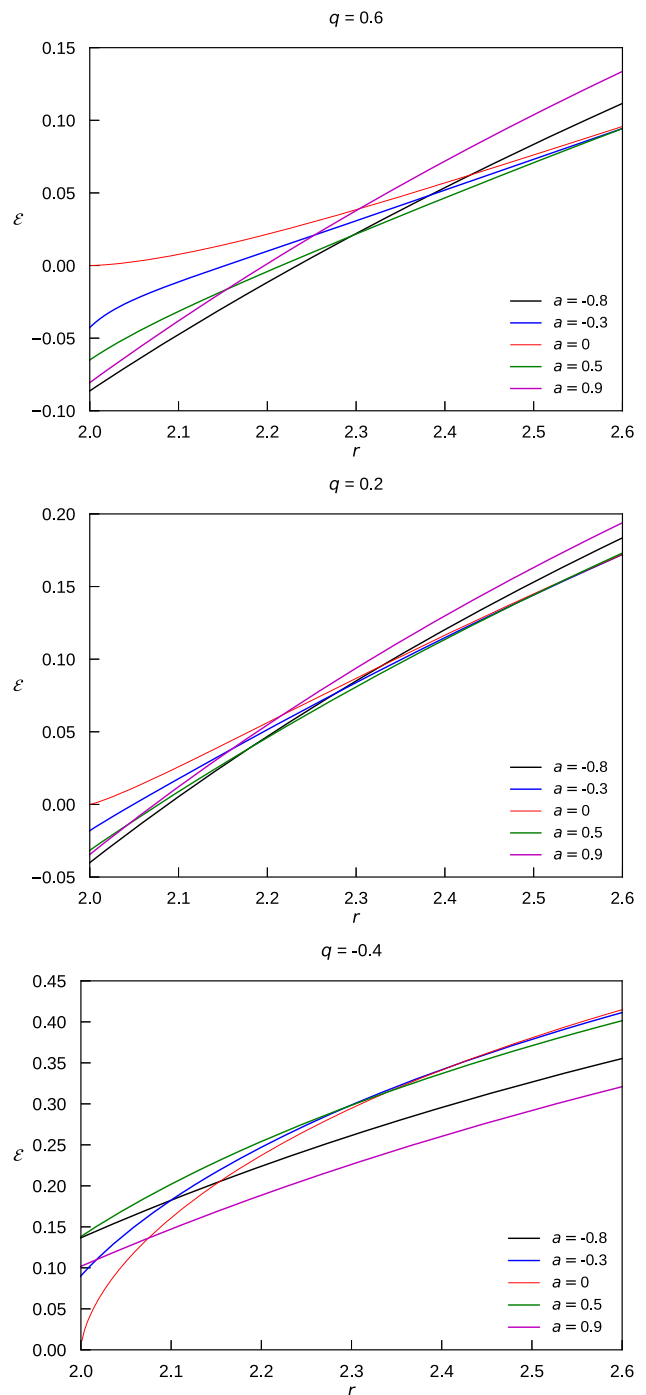


Fig. 4 The Ernst potential, \mathcal{E} , is depicted for various values of q and a

and a shape that depends on the coordinate θ and on the value of the quadrupole parameter q .

One would expect that in the space-time of the stationary q -metric, the singularity structure is affected by the presence of the rotation parameter a . To see this, we examine the

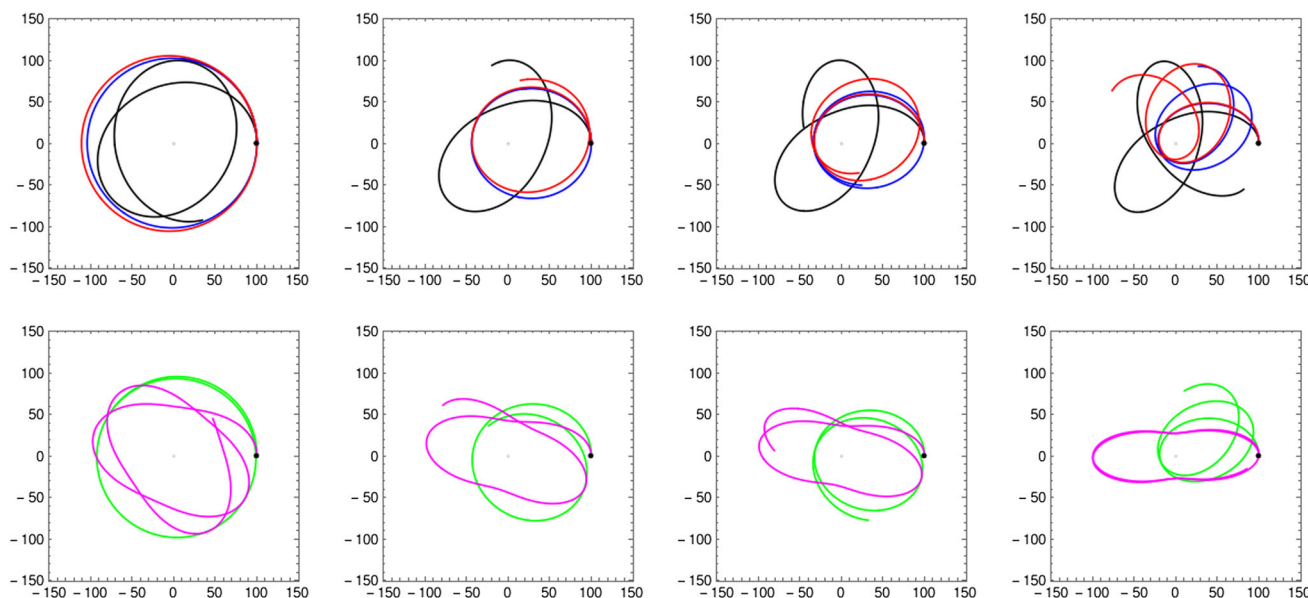


Fig. 5 Bounded trajectories for various combinations of a and q . The first row is dedicated to $a \leq 0$ and the second one to $a > 0$. The colors refers to the values of a following the same code as the Fig. 5. From

the left to the right $q = -0.4, q = 0, q = 0.2$ and $q = 0.6$. All along the plots the following parameters remain constant: The angular momentum $L = 8$, the initial point $r(0) = 100$, and $\phi(0) = 0$

behavior of the Kretschmann scalar

$$\mathcal{K} = R_{\nu\mu\tau\theta} R^{\nu\mu\tau\theta}, \tag{26}$$

in this space-time. However, the complexity of the metric (2) prohibits us to express the Kretschmann scalar explicitly. Therefore, we perform a careful numerical evaluation and analytical inspection to see whether the Kretschmann scalar can be singular for different choices of parameters of the metric on the equatorial plane.

The analysis of the Kretschmann scalar shows that also in the spinning case, for any $q \neq 0$ the hypersurface $r = 2m$ is always singular, besides the curvature singularity located at $r = 0$. Inside the radius $r = 2m$, several singular structures can exist depending on the value of q and a , meaning that there are inner singularities located inside the outer singular hypersurface $r = 2m$. In addition, as the magnitude of the rotation parameter $|a|$ decreases, the location of the inner singularities approach the outer singular hypersurface $r = 2m$, and no singularities were found outside the radius $r = 2m$. To sum up, for the asymptotic behavior of the Kretschmann scalar, we found that a curvature singularity is at $r = 0$ independently of the value of q and a . Besides, there are two situations: If $q = 0$ and $a \neq 0$ also there is a ring singularity at $r = a$. And if $q \neq 0$ by increasing $|a|$, the radius of the singularities decreases and always lay inside this hypersurface $r = 2m$.

It is worth mentioning that in the absence of both q and a we recover the Schwarzschild metric with the only curvature singularity is at $r = 0$. In addition, in the limit $q = 0, a \neq 0$,

one can recover the Kerr metric in Boyer–Lindquist coordinates after applying an algebraic Ehlers transformation, at the level of the Ernst potential. The details of this procedure are outside the scope of this work and will be presented elsewhere. However, it does not affect the local singularity properties of the space-time [37, 39] and the results still valid.

Since we are interested in studying Thick disks that are far away from the hypersurface $r = 2m$, the intersection points are not an obstacle for the investigation of the disks physical properties.

3.4 On the existence of bounded trajectories

The main goal of this work is to investigate the structure of equipotential surfaces of the Thick accretion disk model. To do so, the first step after studying the space-time itself is to examine if bounded and circular trajectories are possible in this background.

In general, the trajectory of a test particle in the background of the stationary q -metric is chaotic. However, trajectories that are close to the minima of the effective potential, representing stable circular orbits, have a regular character [42–45]. Here, as mentioned before, we focus on the existence of the regular bounded and circular orbits located on the equatorial plane.

The expression for the effective potential in this background is rather large and complicated. In general, however, as a standard procedure related to the behavior of the effective potential, one can distinguish four different types of energetic

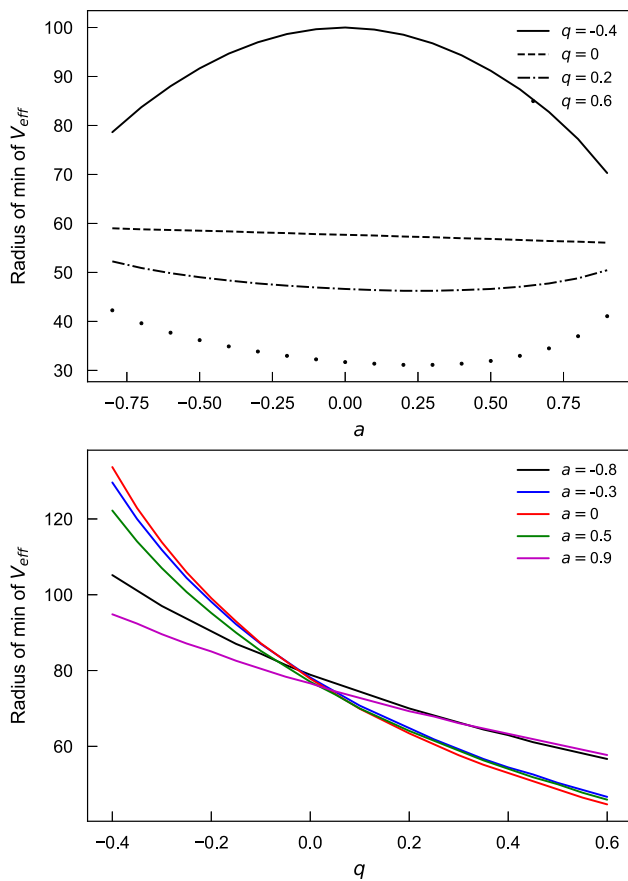


Fig. 6 Top: Minimum of the effective potential versus a for fixed q . Bottom: Minimum of the effective potential versus q for fixed a . The value of L is the same for each plot

boundaries. First, in the case that no inner and outer boundaries exist, the particle can either fall onto the central object or escape to infinity. Secondly, if there exists only one of these boundaries, the particle must fall into the strong gravitational field of the central object or must escape to infinity. Finally, when both inner and outer boundaries exist, the particles are trapped and form a toroidal region in the vicinity of the compact object. Therefore, by examining the last case, where bounded orbits are possible, we investigate the possibility of having disk configurations. An example of such trajectories is illustrated in Fig. 5 for several values of the quadrupole q and the rotation a . Another important particular case is that of circular geodesics, which correspond to the situation when the effective potential equals the specific energy of the particle $V_{\text{eff}}^2 = E^2$. Where the effective potential of the particle motion in (t, r, θ, ϕ) coordinates takes this form

$$V_{\text{eff}}(r, \theta) = \frac{g^{t\phi}L - \sqrt{L^2((g^{t\phi})^2 - g^{tt}g^{\phi\phi}) - g^{tt}}}{g^{tt}}. \quad (27)$$

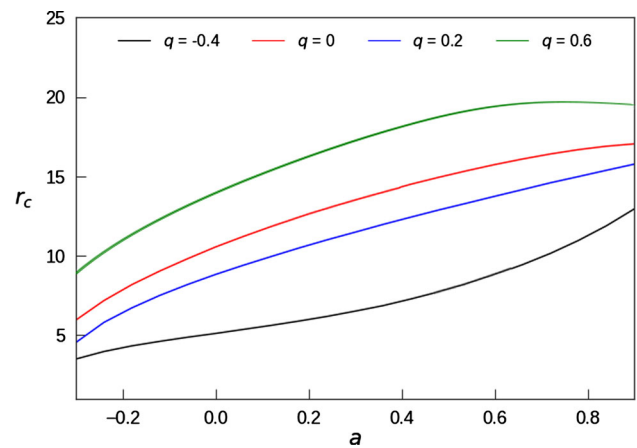


Fig. 7 The variation of the position of the center of the disk as a function of a

The existence of stable circular orbits requires having a minimum in the effective potential. However, the expression of effective potential in this background is rather large and complicated to be treated analytically. Therefore, we employed numerical analysis which indicates that for a large range of the parameters with fixed values of the specific energy E and angular momentum L , the minimum exists; however, the place of the minimum depends on the value of the parameters of the metric. For instance, Fig. 6 shows the place of the effective potential minimum as a function of the parameter a (top panel) and as a function of parameter q (bottom panel). We have seen that circular geodesics are possible in the entire range of parameter values that we used in this work.

Our results show that indeed in the gravitational field of the stationary q -metric bounded orbits are allowed, which can be interpreted as indicating the existence of accretion disks around the source. Thus, in the next section, we explore the possibility of constructing models for Thick disks on the background of the stationary q -metric.

4 Profile of the toroidal disk

The model of equilibrium tori for accretion disks is characterized by a negligible loss of mass and no self-gravity. In these models, the gravity plays a crucial role in building the equipotential configurations. One of the important features of the tori model is that it exhibits locally a stabilizing mechanism against thermal and viscous instabilities, and globally versus the Papaloizou and Pringle instability [46,47]. In these configurations, the equation of state corresponds to that of a barotropic perfect fluid since the model is based on the Boyer’s condition. Moreover, the fluid does not influence the space-time background and it is considered as test matter. To briefly explain this model, we proceed as follows. The general stationary axisymmetric metric in the spherical-like

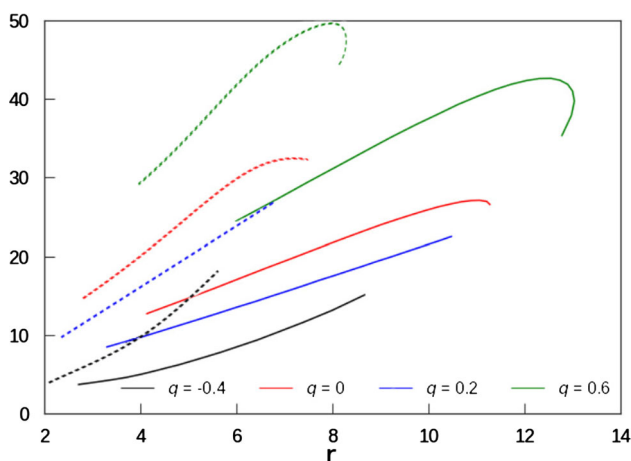


Fig. 8 The variation of ℓ_{mb}^2 (dashed line) as a function of r_{mb} , and the variation of ℓ_{ms}^2 (thick line) as a function of r_{ms} . Besides, the places of r_{mb} and r_{ms} also change with varying q and a . From the left to the right for each curve, a goes from negative to positive values

coordinates is given by

$$ds^2 = g_{tt}dt^2 + 2g_{t\phi}dtd\phi + g_{rr}dr^2 + g_{\theta\theta}d\theta^2 + g_{\phi\phi}d\phi^2, \tag{28}$$

where $g_{\mu\nu} = g_{\mu\nu}(r, \theta)$. The stress-energy tensor contains only the contribution of the perfect fluid; therefore, we have

$$T^\mu{}_\nu = wu^\mu u_\nu - \delta^\mu{}_\nu p, \tag{29}$$

where p is the pressure, w is the enthalpy as measured by an observer moving with the fluid, and the four velocity u^μ is given by $u^\mu = (u^t, 0, 0, u^\phi)$ since we assume that the fluid rotates in the azimuthal direction.

In this model, it is assumed that the angular velocity of the rotating fluid Ω is a function of the angular momentum ℓ per unit mass [48], $\Omega = \Omega(\ell)$, where

$$\Omega = -\frac{g_{t\ell} + g_{t\phi}}{g_{t\phi}\ell + g_{\phi\phi}}, \tag{30}$$

where $\ell = \frac{L}{E}$ ¹. Finally, considering the assumptions of the model, the continuity equation, and the conservation of the stress-energy tensor, the equation of motion of the fluid, i.e., the relativistic Euler equation for the circular motion, can be written in terms of surfaces of constant pressure, equipotential surfaces W , as follows [48]

¹ Normally a constant of geodesic motion in axially symmetric space-times is defined as only the nominator L . However, for having pressure, specific enthalpy times L will be a constant of motion. For axially symmetric and stationary space-times the above relation is constant of motion.

$$\int_{p_{in}}^p \frac{dp}{w} = W_{in} - W \tag{31}$$

$$= -\ln \frac{|u_t|}{|(u_t)_{in}|} + \int_{\ell_{in}}^\ell \frac{\Omega d\ell}{1 - \Omega\ell}, \tag{32}$$

where the index “in” refers to the internal edge of the disk. In this case, the general relativistic version of the von Zeipel theorem is fulfilled. Accordingly, the surfaces of equal Ω , ℓ , p and w all are the same [48]. Hence, for the constant angular momentum distribution ℓ_0 , the total potential can be found as

$$W(r, \theta) = \frac{1}{2} \ln \left| \frac{g_{t\phi}^2 - g_{tt}g_{\phi\phi}}{g_{\phi\phi} + 2\ell_0 g_{t\phi} + \ell_0^2 g_{tt}} \right|, \tag{33}$$

This model can be adjusted for both the constant and non-constant angular momentum distributions. For constant angular momentum profile that we adapted here, W fulfills the following conditions [48],

$$\text{surfaces are } \begin{cases} \text{closed,} & \text{if } |\ell_{ms}| < |\ell_0| < |\ell_{mb}|, \\ \text{open,} & \text{if } |\ell_0| \geq |\ell_{mb}|. \end{cases} \tag{34}$$

and if $|\ell_0| = |\ell_{ms}|$, we end up with just a ring. Here ℓ_{mb} and ℓ_{ms} stay for the value of angular momentum at marginally bound and at marginally stable orbits, respectively. Thus, for a perfect fluid matter rotating around an object described by the stationary q-metric, the shapes and location of the equipressure surfaces follow from the specified angular momentum distribution ℓ . In this work, we consider adiabatic disks with negligible influence of radiation. We assume a perfect fluid obeying

$$p = K\rho^{1+\frac{1}{n}} \tag{35}$$

where K is the adiabatic constant, and n is the adiabatic index. Without loss of generality, we assume $n = 3$ for the following calculations. In addition, the cusp point, r_{cusp} , is located at the smallest intersection radius of ℓ_0 and the Keplerian angular momentum, whereas the largest intersection characterizes the center of the disk r_c . At these two points the fluid can move freely as the pressure gradient vanishes. The radius r_c is shown in Fig. 7 as a function of a for different values of q . We see that r_c is an increasing function of a and q . It means that for any fixed value of q (or a), for larger values of a (or q) the disk can be constructed farther away from the central object. In addition, the plots of r_c as a function of a have a maximum for positive q s and a minimum for negative q s. This means that for positive values, if one continuously increases a , the disk configuration shifted from the central source and then come closer. It could be either an interesting behavior of this space-time, or some signal to discard very

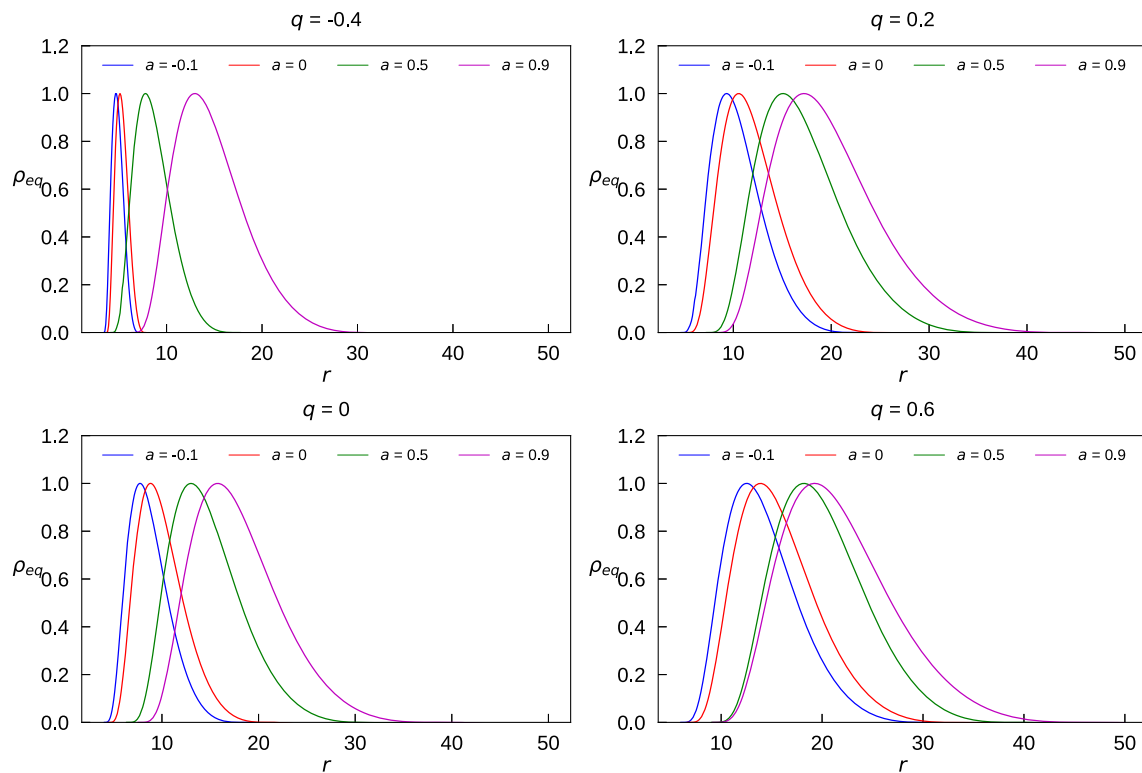


Fig. 9 Density profile on the equatorial plane for different values of parameters q and a . The plots are scaled at each case by the value at the center

large positive values of q . This analysis is beyond the scope of the current work because it would imply a deeper investigation of the physical properties of the background metric.

In Fig. 8, we plot the square of the specific angular momentum at the marginally stable r_{ms} and marginally bound r_{mb} radii for different values of q and a . As mentioned earlier, to have closed equipressure surfaces (34), we need to choose ℓ_0 between the two curves for each model.

In fact, the angular momentum profiles ℓ_{mb}^2 and ℓ_{ms}^2 and their orbits r_{mb} and r_{ms} , as shown in Fig. 8, have the same behavior as r_c with respect to parameters a and q .

In addition, the area between these two profiles also increases, leading to the appearance of a wider region, where closed equipotential surfaces can exist because the chosen angular momentum ℓ_0 should be within this region. A consistent approach for choosing this profile for different values of parameters consists in fixing the constant angular momentum a $\ell_0^2 = \frac{1}{2}(\ell_{mb}^2 + \ell_{ms}^2)$ for all the models.

To see the impact of the parameter a , in Fig. 9, we plot the rest-mass density profiles on the equatorial plane for different values of a and each chosen value for q . We see that as q or a increases, the maximum of the rest-mass density shifts farther away from the central object, which is consistent with the results of Figs. 7 and 8.

To study the influence of the parameters q and a on the pressure, Fig. 10 shows the pressure profiles on the equato-

rial plane. In this figure, we consider both cases of relativistic and non-relativistic gas to see the differences as well as the impact of parameters of the metric on both cases. Following our choice for an adiabatic pressure-mass density relation (35), the energy density is given by $\epsilon = \rho + np$ [49]. However, in the non-relativistic limit one can assume the rest-mass density is sufficiently lower than the contribution of the specific internal energy, $p \ll \rho$. Nevertheless, this difference is very small and it is not possible to detect the deviation on the panels of disk configurations as shown in Fig. 11. However, increasing q or a causes a sharper deviation as seen in Fig. 10.

In Fig. 11, a comparison among the different rows tells us about the role of the quadrupole q for any chosen a , while a contrast among the columns shows the influence of the parameter a on the model for any chosen value of q . Clearly, one can see that by increasing the value of a , the disk moves away from the compact object. Besides, the disk shape becomes extended in the radial direction. A similar pattern is obtained for larger values of q s. Then, both parameters seem to have the same effect on the disk structure. However, a deeper analysis reveals that the growth rate caused by increasing a is higher than by increasing q . For the case $a = 0$ the result is in good agreement with the results found in [16] for a constant angular momentum. Furthermore, in the second column and row, the Schwarzschild case is plotted and we see

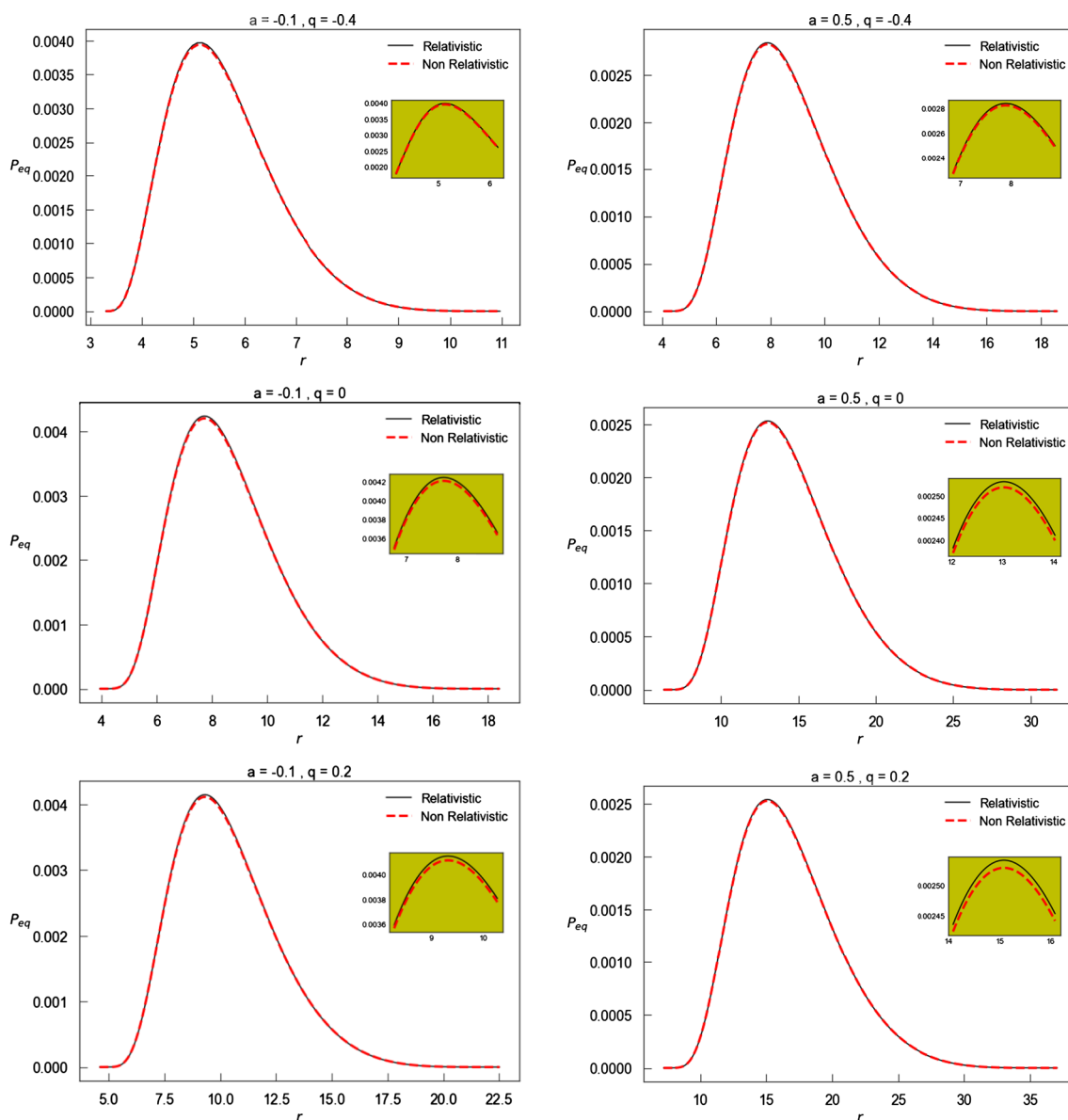


Fig. 10 Pressure profile on the equatorial plane comparing the relativistic and the non-relativistic cases

that by changing these parameters, the configuration of the disk smoothly deviate from this particular choice $a = 0 = q$.

In conclusion, with respect to the central source, the size and position of the disk are a monotonically increasing functions of both parameters a and q . Therefore, it seems reasonable by considering the properties and the overall structure of a Thick accretion disk, one may estimate the rotation and quadrupole parameters of the central compact object at least to find upper and lower bounds on them. For the sake of comparison, Figs. 12 and 13 shows the disk profile for some chosen values of spin parameter a in Kerr and in naked Kerr, respectively. Although the stationary q -metric has a singularity at the horizon, interestingly, the configuration of the accretion disk in this space-time is more similar to the Kerr

configurations rather than the naked Kerr singularity. In particular, for the chosen parameters in both cases we have the cusp. The only difference is by increasing a in Kerr, one obtains a smaller disk structure contrary to the stationary q -metric. On the other hand, the size of the disks by increasing a is similar to the behaviour of disks by increasing a in naked Kerr singularities. Therefore, without testing the hypothesis of the Kerr solution first, it is difficult to distinguish between the Kerr and some other alternatives in astrophysical systems like the Thick accretion disk model.

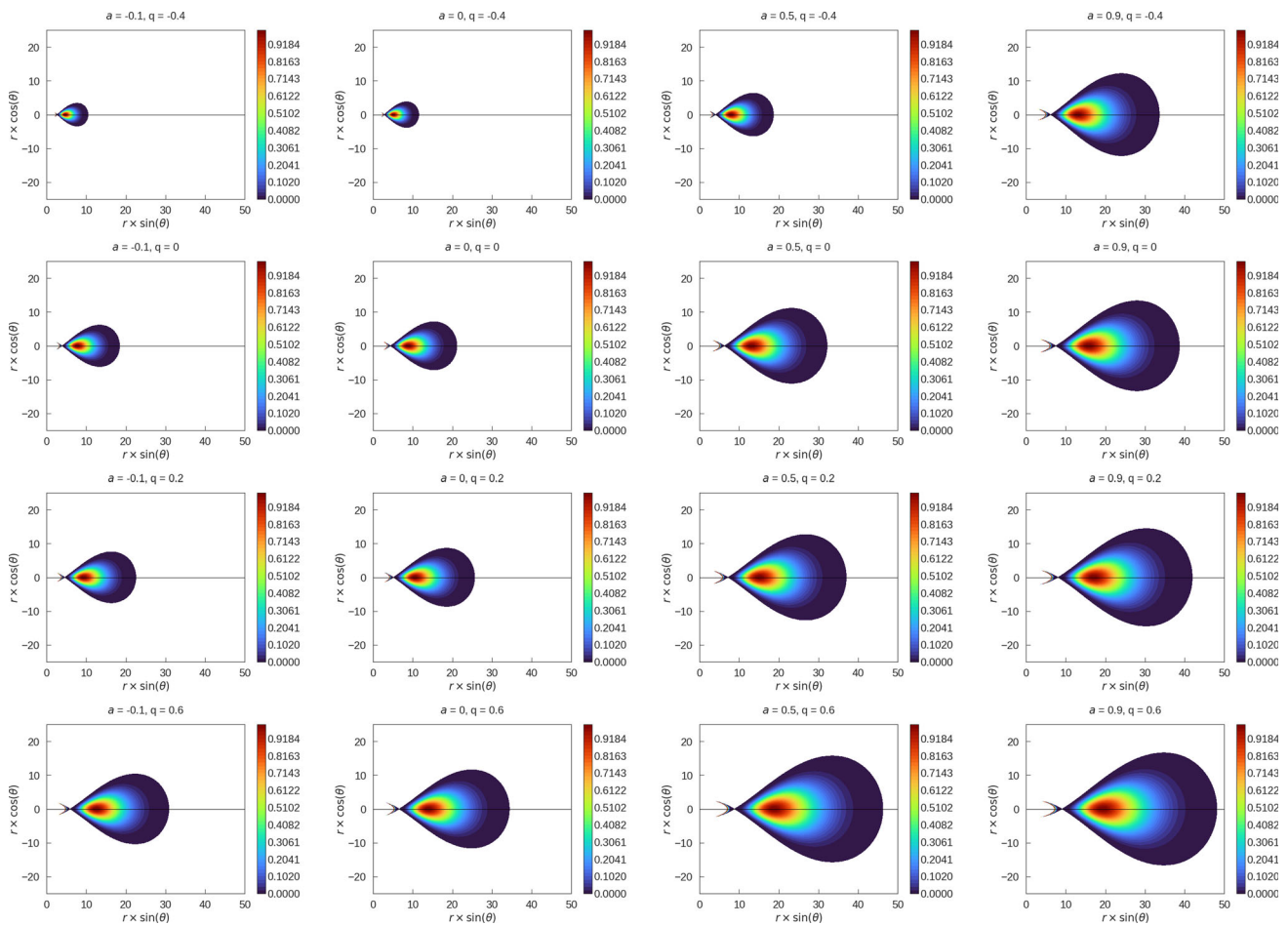


Fig. 11 Equidensity surfaces for various values of a (in column) and q (in row) considered in Fig. 9, in the stationary q -metric

5 Conclusions and summary

In this paper, we analyzed the motion of particles in the stationary q -metric considering relatively small quadrupole q .

We also investigated the structure of Thick disks on this background to reveal the physical properties of this space-time. In particular, we studied the shape and properties of the equipressure surfaces of the Thick disk model. In addition, we compare the results of our analysis with the limiting cases of the static q -metric and the Schwarzschild metric.

In the first part of this work, we analyzed the properties of the Ernst potential as well as the effective potential of the stationary q -metric on the equatorial plane. Interestingly, it turns out that there are certain points very close to $r = 2m$ on the equatorial plane at which the Ernst potential has the same value for different values of a , indicating a sort of degeneracy of the gravitational field at the intersection points. However, this degeneracy does not affect the structure of the accretion disks that are always located far away from these intersections.

In the second part, we explore the structure of Thick tori in the space-time of the stationary q -metric. In general, the parameters q and a drastically affect the shape of the disk. Indeed, the larger the values of q and a , the larger the disk configuration, with an extended shape along the radial direction, and the farther away from the central object is the disk located. These results show that, in principle, it should be possible to determine the rotational and quadrupole parameters of the central object by measuring the shape and location of accretion disks. In addition, we compared our results with those obtained for the Kerr spacetime, including the limit of a naked singularity. It would be interesting to continue the investigation of this space-time by studying the behavior of other astronomical systems that could exist in the gravitational field of the stationary q -metric. In particular, to test the applicability of this solution in the numerical setups and compare it with other backgrounds.

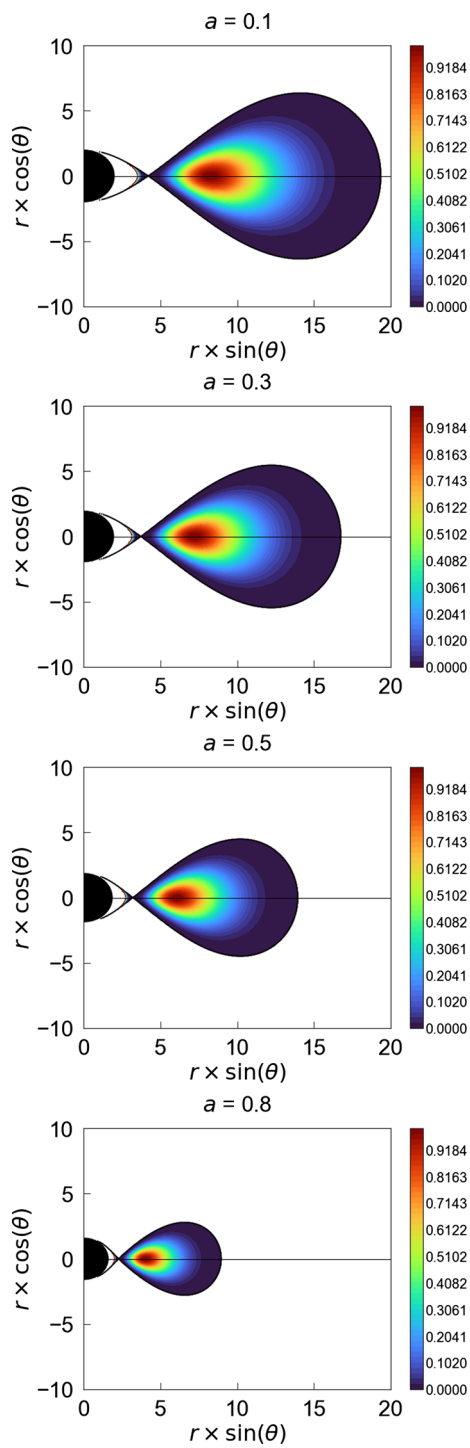


Fig. 12 Equidensity surfaces for various values of a in the Kerr metric

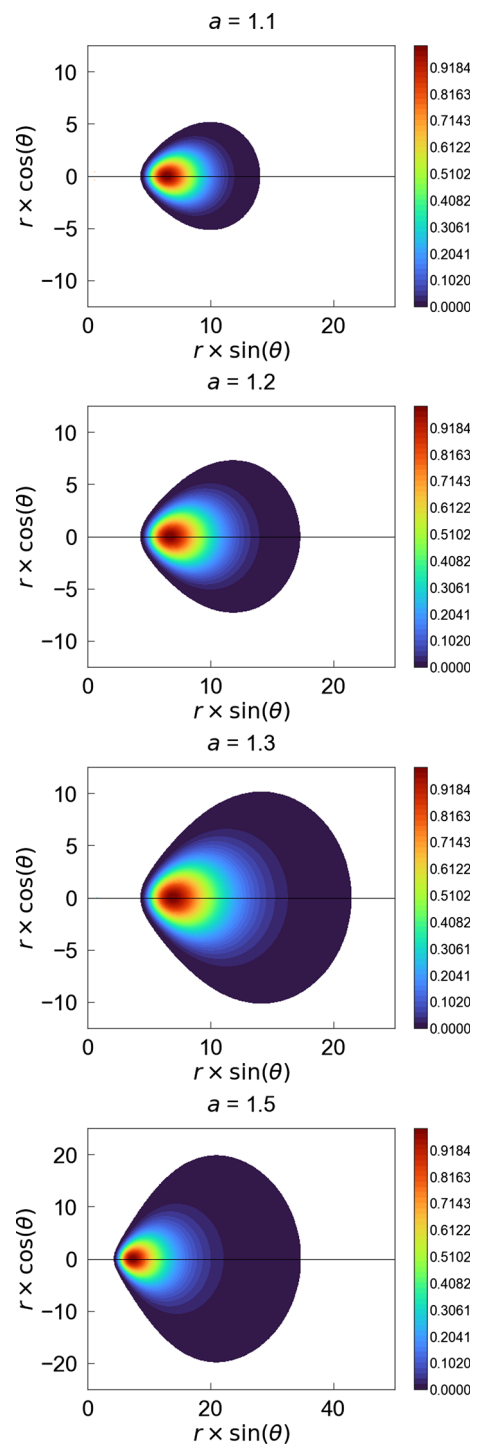


Fig. 13 Equidensity surfaces for various values of a in the naked Kerr singularity

Acknowledgements The authors thank the anonymous referee for the remarks which promoted the work. S.F. thanks the Cluster of Excellence EXC-2123 Quantum Frontiers – 390837967 and the research training group GRK 1620 “Models of Gravity”, founded by the German Research Foundation (DFG). A.T. thanks the research training group GRK 1620 “Models of Gravity”, funded by DFG. H.Q. thanks to UNAM-DGAPA-PAPIIT, Grant No. 114520, and Conacyt-Mexico, Grant No. A1-S-31269.

Data Availability Statement This manuscript has no associated data or the data will not be deposited. [Authors’ comment: No new data were generated or analyzed in this research.]

Open Access This article is licensed under a Creative Commons Attribution 4.0 International License, which permits use, sharing, adaptation, distribution and reproduction in any medium or format, as long as you give appropriate credit to the original author(s) and the source, provide a link to the Creative Commons licence, and indicate if changes were made. The images or other third party material in this article are included in the article’s Creative Commons licence, unless indicated otherwise in a credit line to the material. If material is not included in the article’s Creative Commons licence and your intended use is not permitted by statutory regulation or exceeds the permitted use, you will need to obtain permission directly from the copyright holder. To view a copy of this licence, visit <http://creativecommons.org/licenses/by/4.0/>.

Funded by SCOAP³. SCOAP³ supports the goals of the International Year of Basic Sciences for Sustainable Development.

References

- R. Geroch, Multipole moments. I. Flat space. *J. Math. Phys.* **11**(6), 1955–1961 (1970)
- R. Geroch, Multipole moments. II. Curved space. *J. Math. Phys.* **11**(8), 2580–2588 (1970)
- R.O. Hansen, Multipole moments of stationary space-times. *J. Math. Phys.* **15**(1), 46–52 (1974)
- R.P. Kerr, Gravitational field of a spinning mass as an example of algebraically special metrics. *Phys. Rev. Lett.* **11**(5), 237 (1963)
- M. Heusler, Black hole uniqueness theorems (1996)
- F. Frutos-Alfaro, H. Quevedo, P.A. Sanchez, Comparison of vacuum static quadrupolar metrics. *R. Soc. Open Sci.* **5**(5), 170826 (2018)
- H. Quevedo, Mass quadrupole as a source of naked singularities. *Int. J. Mod. Phys. D* **20**(10), 1779–1787 (2011)
- D.M. Zipoy, Topology of some spheroidal metrics. *J. Math. Phys.* **7**(6), 1137–1143 (1966)
- B.H. Voorhees, Static axially symmetric gravitational fields. *Phys. Rev. D* **2**(10), 2119 (1970)
- K. Boshkayev, E. Gasperin, A.C. Gutierrez-Pineros, H. Quevedo, S. Toktarbay, Motion of test particles in the field of a naked singularity. *Phys. Rev. D* **93**(2), 024024 (2016)
- H. Quevedo, S. Toktarbay, A. Yerlan, Quadrupolar gravitational fields described by the q -metric. arXiv preprint [arXiv:1310.5339](https://arxiv.org/abs/1310.5339) (2013)
- M. Abishev, K. Boshkayev, H. Quevedo, S. Toktarbay, Accretion disks around a mass with quadrupole. In *Gravitation, Astrophysics, and Cosmology: Proceedings of the Twelfth Asia-Pacific International Conference on Gravitation, Astrophysics, and Cosmology*, pp. 185–186 (World Scientific, Singapore, 2016)
- K. Boshkayev, T. Konysbayev, E. Kurmanov, O. Luongo, D. Malafarina, H. Quevedo, Luminosity of accretion disks in compact objects with quadrupole. arXiv preprint [arXiv:2106.04932](https://arxiv.org/abs/2106.04932) (2021)
- J.A. Arrieta-Villamizar, J.M. Velázquez-Cadavid, O.M. Pimentel, F.D. Lora-Clavijo, A.C. Gutiérrez-Piñeres, Shadows around the q-metric. *Class. Quantum Gravity* **38**(1), 015008 (2020)
- M. Abishev, N. Beissen, F. Belissarova, K. Boshkayev, A. Mansurova, A. Muratkhani, H. Quevedo, S. Toktarbay, Approximate perfect fluid solutions with quadrupole moment. *Int. J. Mod. Phys. D* **30**(13), 2150096 (2021)
- S. Faraji, A. Trova, Magnetised tori in the background of a deformed compact object. *Astron. Astrophys.* **654**, A100 (2021)
- S. Faraji, Circular geodesics in a new generalization of q-metric. *Universe* **8**(3), 195 (2022)
- S. Faraji, A. Trova, Quasi-periodic oscillatory motion of particles orbiting a distorted. Deformed compact object. *Universe* **7**(11), 447 (2021)
- S. Faraji, A. Trova, Dynamics of charged particles and quasi-periodic oscillations in the vicinity of a distorted, deformed compact object embedded in a uniform magnetic field. *MNRAS* (2022)
- S. Toktarbay, H. Quevedo, A stationary q-metric. *Gravit. Cosmol.* **20**(4), 252–254 (2014)
- M.A. Abramowicz, Theory of level surfaces inside relativistic: rotating stars. II. *Acta Astron.* **24**, 45 (1974)
- L.G. Fishbone, V. Moncrief, Relativistic fluid disks in orbit around Kerr black holes. *APJ* **207**, 962–976 (1976)
- M. Kozłowski, M. Jaroszynski, M.A. Abramowicz, The analytic theory of fluid disks orbiting the Kerr black hole. *Astron. Astrophys.* **63**(1–2), 209–220 (1978)
- M. Jaroszynski, M.A. Abramowicz, B. Paczynski, Supercritical accretion disks around black holes. *Acta Astron.* **30**(1), 1–34 (1980)
- B. Paczyński, P.J. Wiita, Thick accretion disks and supercritical luminosities. *Astron. Astrophys.* **500**, 203–211 (1980)
- M.A. Abramowicz, M. Calvani, L. Nobili, Thick accretion disks with super-Eddington luminosities. *APJ* **242**, 772–788 (1980)
- B. Paczynski, Thick accretion disks around black holes (Karl-Schwarzschild-Vorlesung 1981). *Mitteilungen der Astronomischen Gesellschaft Hamburg* **57**, 27 (1982)
- B. Paczynski, M.A. Abramowicz, A model of a thick disk with equatorial accretion. *APJ* **253**, 897–907 (1982)
- F. de Felice, Repulsive phenomena and energy emission in the field of a naked singularity. *Astron. Astrophys.* **34**, 15 (1974)
- Z. Stuchlík, Evolution of Kerr naked singularities. *Bull. Astron. Inst. Czech.* **32**, 68 (1981)
- G. Török, Z. Stuchlík, Radial and vertical epicyclic frequencies of Keplerian motion in the field of Kerr naked singularities. Comparison with the black hole case and possible instability of naked-singularity accretion discs. *Astron. Astrophys.* **437**(3), 775–788 (2005)
- M. Kološ, Z. Stuchlík, Dynamics of current-carrying string loops in the Kerr naked-singularity and black-hole spacetimes. *PRD* **88**(6), 065004 (2013)
- C. Chakraborty, P. Kocherlakota, M. Patil, S. Bhattacharyya, P.S. Joshi, A. Królak, Distinguishing Kerr naked singularities and black holes using the spin precession of a test gyro in strong gravitational fields. *Phys. Rev. D* **95**, 084024 (2017)
- D. Charbulák, Z. Stuchlík, Spherical photon orbits in the field of Kerr naked singularities. *Eur. Phys. J. C* **78**(11), 879 (2018)
- M. Rizwan, M. Jamil, K. Jusufi, Distinguishing a Kerr-like black hole and a naked singularity in perfect fluid dark matter via precession frequencies. *Phys. Rev. D* **99**, 024050 (2019)
- D. Bhattacharjee, Solutions of Kerr black holes subject to naked singularity and wormholes (2020)
- H. Quevedo, Multipole moments in general relativity-static and stationary vacuum solutions-. *Fortsch. Phys./Prog. Phys.* **38**(10), 733–840 (1990)
- F. Frutos-Alfaro, M. Soffel, On relativistic multipole moments of stationary space-times. *R. Soc. Open Sci.* **5**(7), 180640 (2018)

39. H. Stephani, D. Kramer, M. MacCallum, C. Hoenselaers, E. Herlt, *Exact Solutions of Einstein's Field Equations* (Cambridge University Press, Cambridge, 2009)
40. F.J. Ernst, New formulation of the axially symmetric gravitational field problem. *Phys. Rev.* **167**, 1175–1178 (1968)
41. F.J. Ernst, New formulation of the axially symmetric gravitational field problem. II. *Phys. Rev.* **168**, 1415–1417 (1968)
42. A.N. Kolmogorov, On conservation of conditionally periodic motions for a small change in Hamilton's function. *Dokl. Akad. Nauk SSSR* **98**, 527–530 (1954)
43. J. Möser, On invariant curves of area-preserving mappings of an annulus. *Nachr. Akad. Wiss. Göttingen* **II**, 1–20 (1962)
44. V.I. Arnol'd, Proof of a theorem of A.N. Kolmogorov on the invariance of quasi-periodic motions under small perturbations of the hamiltonian. *Russ. Math. Surv.* **18**(5), 9–36 (1963)
45. C.W. Misner, K.S. Thorne, J.A. Wheeler, *Gravitation* (1973)
46. M.A. Abramowicz, Innermost parts of accretion disks are thermally and secularly stable. *Nature* **294**(5838), 235–236 (1981)
47. O.M. Blaes, Stabilization of non-axisymmetric instabilities in a rotating flow by accretion on to a central black hole. *MNRAS* **227**, 975–992 (1987)
48. M. Abramowicz, M. Jaroszynski, M. Sikora, Relativistic, accreting disks. *Astron. Astrophys.* **63**, 221–224, 2 (1978)
49. Z. Stuchlík, P. Slaný, J. Kovář, Pseudo-Newtonian and general relativistic barotropic tori in Schwarzschild–de Sitter spacetimes. *Class. Quantum Gravity* **26**(21), 215013 (2009)